



HAL
open science

Selective metal leaching from technosols based on synthetic root exudate composition

Hussein Kanbar, Zeinab Matar, Ghina Abed-Alhadi Safa, Veronique Kazpard

► **To cite this version:**

Hussein Kanbar, Zeinab Matar, Ghina Abed-Alhadi Safa, Veronique Kazpard. Selective metal leaching from technosols based on synthetic root exudate composition. *Journal of Environmental Sciences*, 2020, 96, pp.85-92. 10.1016/j.jes.2020.04.040 . hal-03317781

HAL Id: hal-03317781

<https://hal.science/hal-03317781v1>

Submitted on 28 Dec 2022

HAL is a multi-disciplinary open access archive for the deposit and dissemination of scientific research documents, whether they are published or not. The documents may come from teaching and research institutions in France or abroad, or from public or private research centers.

L'archive ouverte pluridisciplinaire **HAL**, est destinée au dépôt et à la diffusion de documents scientifiques de niveau recherche, publiés ou non, émanant des établissements d'enseignement et de recherche français ou étrangers, des laboratoires publics ou privés.

1 Selective metal leaching from technosols based on synthetic root exudate composition

2
3 Hussein Jaafar Kanbar^{1,2,**}, Zeinab Matar^{1,3,4,**}, Ghina Safa^{1,3}, Veronique Kazpard^{1,3,4}

- 4
- 5 1. Research and Analysis Platform for Environmental Sciences (PRASE), Doctoral School
6 of Sciences and Technology (EDST), the Lebanese University, P.O. 5, Rafic Hariri
7 Campus, Hadat, Lebanon.
 - 8 2. Department of Chemistry, Umeå University, SE-901 87, Umeå, Sweden.
 - 9 3. Department of Earth and Life Sciences, Faculty of Sciences, the Lebanese University,
10 Rafic Hariri Campus, Hadat, Lebanon.
 - 11 4. Laboratory of Georessources, Geosciences and Environment (L2GE), Faculty of
12 Sciences, the Lebanese University, Fanar, Lebanon.

13 Received 16 February 2020

14 Revised 13 April 2020

15 Accepted 24 April 2020

16

17 **Abstract:** This study focused on metal release from technosols induced by synthetic root
18 exudate (SRE). The effect of SRE composition on metal release was studied using six
19 technosols. This was done by treating the technosols with SRE solutions having varying
20 concentrations of low molecular weight organic acids (LMWOAs), namely oxalic, citric, and
21 malic acids. Consequently, the physico-chemical parameters (pH and electric conductivity), Ca,
22 Mg, Fe, Zn, and Cu release (by atomic absorption spectroscopy, AAS), chemical changes (by
23 Fourier transform infrared, FTIR), and organic parameters (by fluorescence) were investigated.
24 Metal release showed to be dependent on the SRE composition and technosol characteristics.
25 Citric acid selectively released Ca, Mg, Zn, and Cu from technosols in a concentration-
26 dependent manner; oxalic acid showed a significant role in the release of Mg and Fe. Under
27 relatively high LMWOA concentrations, particulate organo-mineral complexes precipitated.
28 Additionally, technosol weathering was seen by the dissolution of humic substances and
29 ferriallophanes, which in turn caused metal release. However, re-precipitation of these phases
30 showed to re-sorb metals, thus underestimating the role of LMWOAs in metal release.
31 Therefore, the selective metal leaching was highly dependent on the SRE composition and
32 LMWOA concentrations on one hand, and on the mineral, organic, and organo-mineral
33 components of the technosols on the other. The understanding of such processes is crucial for

34 proposing and implementing environmental management strategies to reduce metal leaching or
35 for the beneficial re-usage of metals (e.g., for agromining) from technosols.

36

37 **Keywords:**

38 Technosols

39 Oxalic acid

40 Citric acid

41 Metals

42 Desorption

43 Organo-mineral complexes

44

45 -----

46 ** These authors contributed equally to this work. Corresponding authors. E-mail:
47 Hussein.kanbar@umu.se (H.J. Kanbar), z.matar@ul.edu.lb (Z. Matar).

48

49 **Introduction**

50 The production of anthropogenic materials is increasing worldwide due to urbanization and
51 consequent development of industrial activities. This results in the formation of soils rich in
52 organic and inorganic technogenic materials, i.e., technosols (e.g., De Kimpe and Morel, 2000).
53 Studies focusing on the processes that occur in technosols, such as aging (Huot et al., 2013),
54 formation of new minerals or organo-mineral complexes (Huot et al., 2014), and leaching of
55 metals (Kanbar et al., 2018), have been reported in the literature. Moreover, technosol
56 rehabilitation is a beneficial way of dealing with such materials. Indeed, technosols can be used
57 as agricultural amendments (Paz-Ferreiro et al., 2014) or for metal mining via
58 phytomining/agromining (Van der Ent et al., 2018), both resulting in profitable and
59 environmentally safe results. These proposed solutions are based on selective metal extraction,
60 leaching, or uptake (Do Nascimento and Xing, 2006), which in turn depend on complex
61 interactions occurring between technosols and plant exudates (e.g., Badri and Vivanco, 2009).
62 Plants release root exudates to cope in toxic environments by leaching undesirable or potentially
63 harmful metals. Nonetheless, under nutrient-deficiency conditions, root exudates help in
64 nutrient uptake (Chen et al., 2017). Accordingly, either bio-available or non-available metal
65 complexes are formed. The composition and concentration of root exudates depend on the state
66 of the plant, such as age, species, and draught level (Do Nascimento and Xing, 2006). However,
67 root exudates generally contain sugars, amino acids, phenolic acids, and low molecular weight

68 organic acids (LMWOAs). The LMWOAs are the main components involved in metal
69 behavior, mainly citric, succinic, malic, and oxalic acids (Agnello et al., 2014).
70 The behavior of metals or nutrients depends on the physico-chemical, organic, metal, and
71 mineral characteristics of technosols (Kanbar et al., 2018). Weathering of mineral surfaces
72 (Kanbar and Kaouk, 2019) and forming dissolved or particulate organo-mineral complexes
73 (Violante and Caporale, 2015) are some of the processes that depict metal behavior. Therefore,
74 metal behavior in matrices, including technosols, can only be understood by taking into
75 consideration these changes in addition to the SRE characteristics (composition and
76 concentration). Studies that focus on the effect of synthetic root exudate (Huang et al., 2017)
77 and individual LMWOAs, such as oxalic acid and citric acid (Chen et al., 2017; Song et al.,
78 2016), on metal release have been reported in the literature. Nonetheless, rarely are the physico-
79 chemical, mineral, chemical, and organic changes of the matrix linked to SRE composition and
80 concentrations, especially in technosols. Therefore, this study aims to highlight the effects of
81 individual LMWOAs, as part of a complex SRE, on metal behavior in technosols. Additionally,
82 the processes undergoing in the liquid (SRE) and solid phases (technosols) were followed by
83 the physico-chemical, mineral, and organic changes caused by SREs having different LMWOA
84 composition and concentrations. Combining the results of the dissolved and particulate phases
85 will help in understanding the behavior of metals in technosols. Consequently, treatment or the
86 beneficial utilization of technosols, such as mining for precious metals (agromining), will be
87 feasible.

88

89 **1 Materials and methods**

90

91 Metal desorption experiments were conducted on six technosols collected from the Lebanese
92 seashore. The technosols were named NS1, NS4, NS9, FS11, FS14, and FS17. Information
93 about sampling location and treatment, technosol characteristics (physico-chemical, mineral,
94 chemical, and organic), total and oxalate extractable metals, and the role of organic matter on
95 metal behavior are found elsewhere (Kanbar et al., 2018).

96

97 **1.1 Synthetic root exudate composition**

98 Seven synthetic root exudate solutions of various LMWOA concentrations were used to study
99 metal behavior in the technosols. It should be noted that the composition of root exudates and
100 their concentrations largely depend on soil type, nutrient availability, metal toxicity, drought
101 condition, microbiome, plant species, and others (Bowsher et al., 2016). The normal SRE

102 composition used in this study, named “S”, was based on Huang et al. (2017). This SRE was
103 proven to selectively desorb metals (Kanbar and Kaouk, 2019). The other 6 SRE solutions had
104 different concentrations of oxalic acid (OA), citric acid (CA), and malic acid (MA) since these
105 LMWOAs are the main components depicting metal behavior. S_{-OA} and S_{-CA} are similar to S
106 except for the absence of OA and CA, respectively; S_{+OA}, S_{+CA}, and S_{+MA} are similar to S except
107 for 5-fold concentrations of OA, CA, and MA, respectively; S_{5X} is 5 times more concentrated
108 than S. The exact concentrations are included in **Appendix A (Table S1)**.

109

110 **1.2 Metal desorption experiment**

111 Each of the six technosols was treated with seven SRE solutions. A control sample (named Ctr)
112 was run for each technosol using ultrapure water instead of SRE. 50 mL of each SRE solution
113 was added to 200 mg of each technosol. The samples, run as triplicates, were shaken in an end-
114 over-end shaker for 24 hr under ambient room temperature; negative controls were also run
115 (i.e., just SRE solutions). The samples were then filtered using 0.45 µm filters and the pH and
116 EC values were recorded (pH_f and EC_f); the pH and EC of the initial SRE solutions were also
117 recorded (pH_i and EC_i). The pH values are reported as ΔpH (ΔpH= pH_f - pH_i). After the
118 experiment, the technosols were freeze-dried before FTIR analysis (Fourier transform infrared).
119 Furthermore, the filtered solutions were used for fluorescence spectrophotometry, FTIR, and
120 atomic absorbance spectroscopy (AAS). The samples were acidified (by 1% HNO₃) before
121 metal quantification (Ca, Mg, Fe, Zn, and Cu) by AAS (Rayleigh WFX-210; Shimadzu, China).
122 Quality assurance and quality control (QA/QC) procedures are included in **Appendix A (S1)**.

123

124 **1.3 Fourier transform infrared**

125 The chemical changes of the solid (technosols) and liquid (SRE solutions) samples after the
126 metal desorption experiment were determined by FTIR (FTIR-6300, JASCO, USA). The
127 samples were prepared in KBr and the spectra were collected between 4000 and 400 cm⁻¹. The
128 raw FTIR spectra were treated and normalized using the open-source MCR-ALS GUI provided
129 by the Vibration Spectroscopy Core Facility at Umeå University
130 (www.umu.se/en/research/infrastructure/visp/downloads/).

131

132 **1.4 Fluorescence spectroscopy**

133 The organic characteristics of the initial and final SRE solutions were detected by fluorescence
134 spectroscopy (Fluorescence spectrophotometer F-7000, Hitachi, Japan). The spectra were
135 recorded by a Fluorolog fluorescence spectrophotometer equipped with both excitation and

136 emission monochromators. A 150-W Xenon arc lamp was used as the excitation source. A
137 complete representation of the fluorescence spectra was presented in the form of an excitation-
138 emission matrix (EEM). The samples were placed in 1 cm optical path quartz cells and
139 thermostated at 20°C. The 3D fluorescence spectra were obtained by increasing the excitation
140 wavelengths from 240 to 600 nm (5 nm intervals) and emission wavelengths from 320 to
141 550 nm (2 nm intervals). The scan speed was set to 240 nm/min. The parameters were based
142 on Lefevre et al. (2013). The final spectra were produced after subtraction from ultrapure water
143 spectra (blank). The fluorescence intensities are given in arbitrary units.

144

145 **2 Results and discussion**

146 **2.1 Physico-chemical changes induced by SREs**

147 The pH values of the initial SRE solutions depended on the composition and concentrations of
148 the organic acids (based on the pKa values of the carboxyl groups). The pH_f values changed
149 due to the chemical, mineral, and organic composition of the technosols. For example, the pH_f
150 of S_{+OA} treated samples did not show the lowest pH (or ΔpH, **Fig. 1a**) even though OA was the
151 strongest acid among the other LMWOAs (based on pKa, **Table S1**). However, the carboxyl
152 groups of OA deprotonated first. The influence of amino acids and phenolic acids on pH
153 variation was not discussed since their concentrations were similar in all the SRE solutions. The
154 pH_i and pH_f values ranged between 2.7-3.6 and 6-8, respectively (**Table S2**). The pH_f values
155 (or ΔpH) of the technosols treated with relatively high LMWOA concentrations (i.e., S_{+OA},
156 S_{+CA}, S_{+MA}, and S_{5X}) were lower than samples treated with S (**Fig. 1a**). Moreover, there was no
157 direct correlation between pH and LMWOA concentrations. S_{-OA} showed lower ΔpH values in
158 comparison to S_{+OA}, indicating higher acidity for the treatments with lower OA concentrations;
159 the same applied to CA treated samples (i.e., S_{-CA} and S_{+CA}). This unexpected variation might
160 be explained by the formation of organo-mineral complexes, incomplete dissolution or
161 dissociation of the added organic components, or the dissolution of humic substances from the
162 technosols (Agnello et al., 2014; Drever and Vance, 1994) when LMWOA concentrations
163 exceeded a certain limit (2 mmol/L for S_{+OA} and S_{+CA} in this case, **Table S1**). This was further
164 supported by the fact that S_{5X} treated samples did not show the lowest ΔpH values. In general,
165 the different SRE solutions, and not the technosols, explained the variation in pH as well as EC.
166 Unlike pH, EC was linked to the LMWOA concentrations in the SRE solutions (**Fig. S1**).
167 Indeed, the EC_f values increased in the following order: S_{-OA} and S_{-CA} (294-370 μS/cm), S (353-
168 429 μS/cm), S_{+OA}, S_{+MA}, S_{+CA} (368-580 μS/cm), and S_{5X} (715-880 μS/cm) (**Fig. 1b**); the
169 concentrations of the LMWOAs were 0.75, 1, 2, and 5 mmol/L, respectively (**Table S1**). Due

170 to the different processes occurring in the mixture, such as sorption/desorption of metals and or
171 dissolution/precipitation of phases, there was no linear correlation between the LMWOA
172 concentrations and EC. Even though the initial NS technosols had higher electric conductivity
173 than the FS technosols (Kanbar et al., 2018), this was not the case after mixing with the SRE
174 solutions. The initial EC values are included in **Table S2**.

175

176 **2.2 Release of major cations by LMWOAs in a concentration-dependent manner**

177 The release of the major cations, Ca and Mg, varied between the different treatments but not
178 among technosols (**Fig. 2a and b**). The technosols treated with S_{+CA} , S_{+MA} , and S_{5X} had the
179 highest Ca release, partially due to the dissolution of Ca-containing carbonates; the presence of
180 carbonates was proven by X-ray diffraction (Kanbar et al., 2018). Indeed, Oelkers et al. (2011)
181 evidenced that citrate (>0.1 mmol of citrate per kg of carbonate) significantly increased
182 carbonate dissolution. In our case, 0.25 and 1.25 mmol/L of citric acid (S and S_{+CA} ,
183 respectively) showed a significant role in Ca release; this was not seen when CA concentrations
184 were below 0.25 mmol/L (i.e., between S_{-CA} and S). Even though FS17 had the lowest initial
185 Ca content among the other technosols (**Table S3**), it did not show the lowest Ca release,
186 indicating that the initial Ca content is not linked to Ca release in this case. Therefore, and in
187 addition to Ca-carbonate dissolution and incorporated Ca release (e.g., inner-sphere
188 complexes), weakly bound Ca onto mineral and organic/humic surfaces and hydrated Ca was
189 also released by SRE (e.g., Kanbar and Kaouk, 2019). On that note, ultrapure water treated
190 technosols (Ctr) also showed Ca release (~ 0.1 - 0.6%). It is worth noting that Ca release was
191 similar regardless of OA concentration (Ca release for $S_{-OA} \sim S \sim S_{+OA}$). The processes explaining
192 Ca release also applied to Mg. Moreover, S_{+MA} and S_{+CA} treated technosols showed similar
193 contents of Ca and Mg release, possibly due to similar pK_a values (**Table S1**), assuming similar
194 dissociation, carboxyl group deprotonation, and major cation binding. Furthermore, the Mg
195 released contents increased in the following order: S_{-OA} and S_{-CA} , S, S_{+OA} , S_{+CA} , and S_{+MA} , and
196 finally S_{5X} . The metal release was linked to higher conductivity, salinity, and ionic strength
197 (e.g., Du Laing et al., 2009); this was seen in the case of Mg and Ca (**Fig. S1**), but not for the
198 other metals. Finally, Ca release from the technosols was CA and MA-concentration dependent
199 when the LMWOA concentrations were relatively high (1-2 mmol/L), while Mg release was
200 CA and OA-concentration dependent when the LMWOA concentrations ranged between 0.75
201 and 1 mmol/L. The magnitudes of metal release based on the SRE solutions are shown in **Fig.**
202 **S2**.

203

204 2.3 Selective metal leaching from technosols

205 In contrast to the major cations (Mg and Ca), the release of Fe, Zn, and Cu was selective based
206 on the composition of the technosols, SRE solutions, and the metals themselves (**Fig. 2c-e**). On
207 the selectivity of the technosols, the NS samples showed the highest Fe release, the NS samples
208 and FS11 showed the highest Zn release, and NS4 and NS9 showed the highest Cu release. The
209 correlation between the released metals (Fe, Zn, and Cu) are included in **Fig. S1**. In all cases,
210 S_{5X} showed the highest metal release; so, S_{5X} is not concerned in the discussion below. Iron
211 was mainly released by S_{+OA} treatment, while Zn and Cu were mainly released by S_{+CA}
212 treatment. Nonetheless, the other LMWOAs were also involved in the release of Fe, Zn, and
213 Cu. The highest metal release was recorded for samples having the highest total metal and
214 oxalate extractable metal contents. The percentages of the oxalate extractable metals for those
215 samples (marked as bold in **Table S3**) averaged 65%, 66%, and 33%, for Fe, Zn, and Cu,
216 respectively. Ferriallophanes or Fe-oxyhydroxides and oxalate extractable metals were the main
217 causes of high metal release. Indeed, the dissolution of Fe-oxyhydroxides from the Fe-rich
218 technosols was expected after mixing with SREs, even at neutral to alkaline pH (e.g., Chen et
219 al., 2017); additionally, OA was proven to release Fe from Fe-bearing minerals (Pariyan et al.,
220 2019). The effect of OA concentration on Fe release was seen between S_{-OA} and S_{+OA} treatments
221 (i.e., between 0 and 1.25 mmol/L of OA), however, the variation was more prominent in the 0-
222 0.25 mmol/L range ($S/S_{-OA} > S_{+OA}/S$, **Fig. S2**); the same applied to CA. The S and S_{+MA} treated
223 technosols showed similar Fe content release. Interestingly, the absence of either OA or CA
224 showed negligible Fe release in all the technosols (inset of **Fig. 2c**). This raises the question of
225 complementarity between the different LMWOAs in some processes, such as forming available
226 binding sites, binding to mineral/humic surfaces, changing degradation rate, desorbing metals,
227 influencing physico-chemical parameters, and dissolving minerals (e.g., (Ström et al., 2001)).
228 Zinc was highly released from the technosols after SRE treatments, even for samples with
229 relatively low initial Zn contents, namely FS14 and FS17 (inset of **Fig. 2d** and **Table S3**). This
230 was caused by the formation of soluble complexes with dissolved organic matter (DOM) (e.g.,
231 Chen et al., 2017). Zinc release from the Zn-rich technosols (all NS samples and FS11) was due
232 to the predominance of oxalate extractable Zn species (Kanbar et al., 2018). Interestingly, Zn
233 release was OA and CA concentration-dependent in those technosols when the LMWOA
234 concentrations ranged between 0 and 1.25 mmol/L. However, Zn release was more affected by
235 CA than by OA, especially when the LMWOA concentrations were relatively low ($S/S_{-CA} >$
236 S_{+CA}/S ; **Fig. S2**). It was proven that DOM of plant exudates, specifically CA, readily sorb Zn
237 (e.g., Song et al., 2016). Zinc release was similar between S_{+MA} and S_{+OA} treated samples, which

238 was lower than S_{+CA} treated ones. Calcium release, on the other hand, was similar between S_{+MA}
239 and S_{+CA} treated samples. Therefore, the dissociation constants of the LMWOA functional
240 groups were not directly linked to metal leaching in the technosols. Other processes depict metal
241 release, such as the formation of organo-mineral complexes (as mentioned in the previous
242 section).

243 Copper release depended on the LMWOA concentrations and components (**Fig. 2e**). It was
244 proven that Cu has a high affinity for binding to organic components, such as CA (Song et al.,
245 2016). Furthermore, it was shown that an SRE solution, similar to S in this study, desorbed
246 surface-bound copper and dissolved Cu-minerals (Kanbar and Kaouk, 2019). Although not as
247 clear as Zn and Fe release, Cu release was dependent on CA and OA when the LMWOA
248 concentrations ranged between 0 and 1.25 mmol/L; yet it was more prominent in the 0.25-
249 1.25 mmol/L range (**Fig. S2**). Regarding Cu release, MA and OA showed similar effects.
250 Interestingly, Cu release was not LMWOA concentration-dependent in the NS1 and FS
251 technosols. This might be because Cu has a high affinity for binding to OM (Matar et al., 2015),
252 and the relatively low LMWOA concentrations were sufficient to release all extractable Cu.
253 Even though NS4 and NS9 had similar Cu contents (total and oxalate extractable, **Table S3**),
254 the role of LMWOAs on Cu release was more prominent for the former; NS4 showed higher
255 variation in Cu release between S_{-OA} and S_{-CA} on one hand, and S_{+OA} and S_{+CA} on the other.
256 This was linked to higher Fe-oxyhydroxides/ferrihallophanes contents in NS4 (as indicated by
257 high oxalate extractable Fe contents, **Table S3**). Indeed, these iron phases might re-sorb
258 released metals (Grybos et al., 2007), thus underestimating the role of LMWOAs on metal
259 release.

260

261 **2.4 Chemical changes of the technosols after SRE treatment and precipitation of organo-** 262 **mineral complexes**

263 **2.4.1 Technosol FTIR spectra**

264 The SRE-induced chemical changes of the technosols are compared; the FTIR spectra of the
265 initial technosols are found elsewhere (Kanbar et al., 2018). In comparison to the initial
266 technosol, the bands in the 800-450 cm⁻¹ region changed after SRE treatment, as shown by the
267 peaks at 790, 612, and 530 cm⁻¹ (**Fig. 3a**). The S and S_{+OA} treated samples showed significant
268 changes in that region; OA readily sorbed onto soils in general (Jagadamma et al., 2012) and
269 Fe-rich minerals in particular (Bhatti et al., 1998), such as the case of the ferrihallophane-rich
270 technosols. This suggested that the peak deformation in that spectral region was partially caused
271 by OA. Other LMWOAs, such as CA, MA, and succinic acid, have a fingerprint in that region

272 as well (e.g., Huang et al., 2017). Moreover, the bands at 650-450 cm⁻¹ might be due to -CH₂
273 vibration, possibly formed by LMWOAs (Huang et al., 2017) or by chemical interactions
274 between the Al-O groups of aluminosilicates in the technosols (e.g., clays or allophanes) with
275 -CH groups of sugars in the SRE solutions (Bishop et al., 2013). The bands in the 600-400 cm⁻¹
276 ¹ region also indicated Si-O bending vibrations (of silicates, aluminosilicates, and allophanes);
277 these bands strongly rely on the octahedral atom (Madejová et al., 2017). Therefore, changes in
278 the IR spectra in that region suggested mineral weathering caused by LMWOAs (Drever and
279 Vance, 1994). On a similar note, the bands in the 850-600 cm⁻¹ region indicated OH bending
280 vibration of minerals, such as clays. In the case of surface complexation (organo-mineral
281 complex), LMWOAs, such as OA and CA (Hayakawa et al., 2018), can weather minerals,
282 consequently leading to spectral modification in the 850-600 cm⁻¹ region (Madejová et al., 2017
283 and references cited therein).

284 The LMWOAs might cause the release of interlayer or inner-sphere metals from clays or
285 organo-mineral complexes present in the technosols. On the formation of organo-mineral
286 complexes, an ester group (C-O) emerged at 1318 cm⁻¹ in the S_{+OA} and S_{5X} treated samples that
287 had a strong technogenic character (**Fig. 3b**), i.e., NS1, NS4, NS9, and FS11; the other samples
288 had a lithogenic nature (Kanbar et al., 2018). The ester group might have formed in the
289 technosols due to SRE-induced weathering. Since this peak was only detected in samples
290 treated with elevated OA concentrations and in certain technosols, it is believed that alcohol
291 groups in OA weathered the carboxyl groups of humic substances or allophanes. Furthermore,
292 the intensity of the 1729 cm⁻¹ peak increased in all the treatments in comparison to the initial
293 spectrum. Therefore, this peak, indicating carbonyl (C=O) of humic substances or LMWOAs
294 (Huang et al., 2017), might have formed by weathering of the allophane-rich NS technosols,
295 binding of LMWOAs onto technosols, or precipitation of organo-mineral complexes (Markich
296 and Brown, 1999). The change in that peak can also be due to the degradation of the ester band
297 (Arocena et al., 1995). Therefore, the possibly formed ester, as discussed previously, might be
298 directly, yet partially, weathered.

299 The OM peaks at 1400 cm⁻¹ (carboxyl stretching and O-H bending of carboxyl group), 1470-
300 1400 cm⁻¹ (aliphatic C-H bending), 1614 cm⁻¹ (-C-O stretching and O-H bending of humic
301 carboxyl groups), 1640 cm⁻¹ (aromatic C=C stretching), and ~3400 cm⁻¹ (amine (N-H)
302 stretching and OH stretching of humic substances) did not show a trend among the treatments
303 (**Fig. 3b and c**). These peaks changed according to humic substance weathering, water content
304 fluctuation, and organic or organo-mineral complex precipitation (Matar et al., 2015). However,
305 the aliphatic C-H stretching peaks (at 2922 and 2852 cm⁻¹) decreased after suspension with SRE

306 as well as ultrapure water (inset in **Fig. 3c**) suggesting the dissolution, degradation, or
307 weathering of organic matter.

308

309 **2.4.2 FTIR spectra of the SRE solutions after metal desorption**

310 The change in the IR spectra of the liquid samples after the metal desorption experiment marked
311 the chemical changes of the dissolved phases (**Fig. 4**). All the samples and treatments showed
312 a peak at 410 cm^{-1} , except for the S_{-CA} and S_{-OA} treated technogenic samples (i.e., NS samples).
313 Hence, the disappearance of that peak was linked to allophane weathering or degradation when
314 the LMWOA concentrations were relatively low (**Fig. 4a**). The precipitation of organo-mineral
315 complexes from the LMWOAs and technosols was possible when the LMWOA concentrations
316 were above 1 mmol/L (i.e., S_{+OA} , S_{+CA} , and S_{+MA}), thus reducing technosol weathering. Indeed,
317 that would be a reason for higher alkalinity for S_{+OA} , S_{+CA} , and S_{+MA} treated technosols in
318 comparison to the S_{-OA} and S_{-CA} treated ones (**Fig. 1a**). Nonetheless, organo-mineral complexes
319 formed due to LMWOA-induced weathering. The higher EC of the high LMWOA solutions
320 promoted complex formation (Newcomb et al., 2017), while the organic acids remained
321 dissolved in the low LMWOA concentrated solutions. Similar results were found in the 600-
322 400 cm^{-1} region (i.e., modified IR spectra for S_{-OA} and S_{-CA} treated technosols). The change in
323 the IR fingerprint might be due to the dissolution of carbonates or other phases that were
324 involved in buffering the solution. Furthermore, the fate of LMWOAs (e.g., dissolution,
325 precipitation, or complexation) was dependent on several parameters, such as pH, EC, and
326 mineral composition (e.g., Newcomb et al., 2017). This further supported the variation in the
327 FTIR fingerprint for the different SRE-treated technosols. Another peak that emerged in the
328 samples was 1730 cm^{-1} (**Fig. 4b**), possibly belonging to the carboxyl group, and more precisely
329 the carbonyl group of LMWOAs. Once deprotonated, that peak disappeared and was replaced
330 by a 1626 cm^{-1} peak (Iwase et al., 1999). Due to peak overlapping, this could not be verified in
331 our case. However, the 1730 cm^{-1} peak was more prominent in the S_{+OA} , S_{+MA} , and S_{+CA} treated
332 samples, suggesting that a part of these LMWOAs did not deprotonate, possibly due to
333 oversaturation and consequent precipitation or organo-mineral complex formation. It should be
334 noted that the organo-mineral complexes could be of various sizes (i.e., particulate or
335 dissolved). On the same note, the peaks at $1640\text{-}1600\text{ cm}^{-1}$ (C=C, C=O, or C-O of humic
336 substance) and 3400 cm^{-1} (NH or OH of humic substances, **Fig. 4c**) were the lowest for samples
337 treated with high LMWOA concentrations, suggesting that SRE solutions with low LMWOA
338 concentrations had a bigger role in humic acid weathering.

339

340 **2.5 LMWOA-induced changes on DOM and indications of organo-mineral complex**
341 **precipitations: fluorescence**

342 The 3D fluorescence EEM showed changes in two regions after suspension with SRE (**Fig. 5**).
343 The first region showed two peaks, which were roughly centered at the $\lambda_{ex}/\lambda_{em}$ of 245-
344 250/338 nm and 290-295/338 nm. These peaks were attributed to microbial by-product like
345 materials, such as proteins and tryptophan. The second region was located in the $\lambda_{ex}/\lambda_{em}$ of
346 260-420/380-500 nm range and was attributed to humic acid (HA)-like substances (Chen et al.,
347 2003). The maximum fluorescence intensities of these peaks, F_{max} , were obtained at fixed
348 excitation wavelengths and are presented in **Fig. 5e** and **Table S4**. Only the humic acid-like
349 region is discussed hereafter due to the link with the processes undergoing in the technosols.
350 The protrusion of the HA-like region differed between treatments but not between the
351 technosols; therefore, the EEM of one technosol is given (**Fig. 5a-d**). There was an
352 enhancement in the HA-like region for samples treated with relatively high LMWOA
353 concentrations, as seen between S_{-OA} and S (**Fig. 5b-c** and **e**). This supported the role of SRE
354 in technosol weathering and HA release when the LMWOA concentrations were low.
355 Therefore, and similar to LMWOAs, HA had a role in releasing metals from the technosols.
356 The change in the HA-like peaks was less obvious for higher LMWOA concentrations, i.e.,
357 between S and S_{+OA} (**Fig. 5c-d**). Under those conditions, and as suggested by FTIR,
358 precipitation of SRE components and formation of particulate organic matter or organo-mineral
359 complexes occurred.

360

361 **2.6 Discussion: chemical and organic processes occurring in the SRE-technosol mixture**

362 The carboxyl groups of the LMWOAs (in the SRE solutions) deprotonated due to the rise in
363 pH caused by the addition of technosols (**Fig. 1a**). Consequently, the dissolved LMWOAs
364 triggered metal release from the technosols (e.g., Perelomov et al., 2011) or formed particulate
365 or dissolved complexes with minerals, organics, or organo-minerals (Pan et al., 2010). Humic
366 acids were also dissolved from the technosols via SRE-induced weathering or degradation (**Fig.**
367 **5**). Therefore, metals might form dissolved or particulate complexes with LMWOAs and HAs.
368 Having a low carboxyl pKa (**Table S1**), OA was expected to be the first LMWOA to sorb
369 metals. Indeed, OA showed the highest influence on Fe, Zn, and Cu release (**Fig. 2c-e**).
370 However, CA has three carboxyl groups, while each of OA and MA has only two (**Table S1**).
371 This might explain higher Zn and Cu release in S_{+CA} treated technosols in comparison to the
372 other SRE solutions (**Fig. 2**). Interestingly, CA showed a more significant role in metal
373 chelating when OA was absent. This was seen by lower metal release for S_{-CA} treated samples

374 in comparison to S_{-OA} treated ones (e.g., Cu and Zn). Double deprotonation of the carboxyl
375 groups of MA occurred after sorption (Karageorgaki and Ernst, 2014). This indicated that even
376 if CA has more carboxyl groups, MA has the same effect on chelating metals or forming organo-
377 mineral complexes. This applied to the release of Ca, Mg, and Cu. Furthermore, organo-mineral
378 complexes formed when the LMWOA concentrations were high. In those treatments, surface
379 mineral weathering was promoted, leading to prolonged periods of metal release (>24 hr).
380 Therefore, more interactions and processes will change the physico-chemical, chemical,
381 mineral, and organic characteristics of the technosols. Accordingly, metal release continuous
382 as long as the organic components (LMWOAs) are in contact with the technosols.

383

384 **3 Conclusion**

385 The synthetic root exudate-induced changes were studied on technosol characteristics (physico-
386 chemical, mineral, organic, and chemical). Metal release from the technosols depended on the
387 SRE composition (i.e., oxalic, citric, and malic acids), LMWOA concentration, and technosol
388 composition (i.e., metal contents, ferriallylophanes, and humic substances). Indeed, the metal
389 release was highly selective. For example, CA and MA showed significant Ca release only
390 when the LMWOA concentrations were relatively high (S_{+CA} and S_{+MA}), while OA did not have
391 a role in Ca release regardless of concentration. However, Mg release was dependent on OA
392 and CA, mainly when the LMWOA concentrations were relatively low. On the other hand, the
393 release of Fe, Zn, and Cu was more selective, especially between the different technosols. The
394 selectivity of metal leaching by LMWOAs largely depended on the solubility of the LMWOAs
395 and technosol composition. Indeed, organo-mineral complexes formed between the LMWOAs
396 and technosol organic matter (humic materials), minerals, and organo-minerals, especially
397 under relatively high LMWOA concentrations. Furthermore, the released metals, e.g., due to
398 humic acid or ferriallylophane dissolution, might be re-sorbed by the precipitating organo-
399 mineral complexes, therefore underestimating the role of LMWOAs on metal release. These
400 findings highlight the different processes that depict metal behavior in heterogeneous
401 technosols. Only when these notions are understood will it be possible to beneficially re-use
402 technosols in sustainable management plans (e.g., agromining).

403

404 **Acknowledgment**

405 This work was financed by the research grant programs of the Lebanese University (le projet
406 est soutenu par le programme de subvention de la recherche scientifique à l'Université
407 Libanaise). The funding source had no involvement in the study design, writing of the report,

408 and decision to submit the article for publication. We thank Dr. Elias Maatouk (Laboratory of
409 Georessources, Geosciences and Environment, L2GE) for flame photometry and EC
410 measurements and the research assistants of the Research and Analysis Platform for
411 Environmental Sciences (PRASE), namely Ms. Sahar Rihane and Ms. Malak Tofeily (FTIR),
412 Ms. Manal Houhou-Hadada and Mr. Ali Berro (AAS), Ms. Marwa Fouani (Fluorescence), and
413 Ms. Layal Hajjar and Mr. Mohammad Siblani (assistance in laboratory work).

414

415 **Appendix A. Supplementary data**

416 Supplementary data associated with this article can be found in the online version at xxxxxx.

417

418 **References**

- 419 Agnello, A.C., Huguenot, D., Van Hullebusch, E.D., Esposito, G., 2014. Enhanced
420 phytoremediation: A review of low molecular weight organic acids and surfactants used
421 as amendments. *Crit. Rev. Environ. Sci. Technol.* 44(22), 2531–2576.
422 <https://doi.org/10.1080/10643389.2013.829764>.
- 423 Arocena, J.M., Pawluk, S., Dudas, M.J., Gajdostik, A., 1995. In situ investigation of soil organic
424 matter aggregates using infrared microscopy. *Can. J. Soil Sci.* 75(3), 327–332.
425 <https://doi.org/10.4141/cjss95-047>.
- 426 Badri, D. V., Vivanco, J.M., 2009. Regulation and function of root exudates. *Plant, Cell*
427 *Environ.* 32(6), 666–681. <https://doi.org/10.1111/j.1365-3040.2009.01926.x>.
- 428 Bhatti, J.S., Comerford, N.B., Johnston, C.T., 1998. Influence of soil organic matter removal
429 and pH on oxalate sorption onto a spodic horizon. *Soil Sci. Soc. Am. J.* 62(1), 152-158.
430 <https://doi.org/10.2136/sssaj1998.03615995006200010020x>.
- 431 Bishop, J.L., Ethbrampe, E.B., Bish, D.L., Abidin, Z.L., Baker, L.L., Matsue, N., et al., 2013.
432 Spectral and hydration properties of allophane and imogolite. *Clays Clay Miner.* 61(1),
433 57–74. <https://doi.org/10.1346/CCMN.2013.0610105>.
- 434 Bowsher, A.W., Ali, R., Harding, S.A., Tsai, C.J., Donovan, L.A., 2016. Evolutionary
435 divergences in root exudate composition among ecologically-contrasting helianthus
436 species. *PLoS One.* 11(1), 1–16. <https://doi.org/10.1371/journal.pone.0148280>.
- 437 Chen, W., Westerhoff, P., Leenheer, J.A., Booksh, K., 2003. Fluorescence excitation–emission
438 matrix regional integration to quantify spectra for dissolved organic matter. *Environ. Sci.*
439 *Technol.* 37(24), 5701–5710. <https://doi.org/10.1021/es034354c>.
- 440 Chen, Y.T., Wang, Y., Yeh, K.C., 2017. Role of root exudates in metal acquisition and
441 tolerance. *Curr. Opin. Plant Biol.* 39, 66–72. <https://doi.org/10.1016/j.pbi.2017.06.004>.
- 442 De Kimpe, C.R., Morel, J.-L., 2000. Urban soil management: a growing concern. *Soil Sci.*
443 165(1), 31–40.
- 444 Do Nascimento, C.W.A., Xing, B., 2006. Phytoextraction: A review on enhanced metal
445 availability and plant accumulation. *Sci. Agric.* 63(3), 299–311,
446 <https://doi.org/10.1590/S0103-90162006000300014>.
- 447 Drever, J.I., Vance, G.F., 1994. Role of soil organic acids in mineral weathering processes. In:
448 Pittman, E.D., Lewan, M.D. (Eds.). *Organic Acids in Geological Processes*. Springer
449 Berlin Heidelberg, Berlin, Heidelberg, pp. 138–161. [https://doi.org/10.1007/978-3-642-](https://doi.org/10.1007/978-3-642-78356-2_6)
450 [78356-2_6](https://doi.org/10.1007/978-3-642-78356-2_6).
- 451 Du Laing, G., Rinklebe, J., Vandecasteele, B., Meers, E., Tack, F.M.G., 2009. Trace metal

452 behaviour in estuarine and riverine floodplain soils and sediments: A review. *Sci. Total*
453 *Environ.* 407(13), 3972–3985. <https://doi.org/10.1016/j.scitotenv.2008.07.025>.

454 Grybos, M., Davranche, M., Gruau, G., Petitjean, P., 2007. Is trace metal release in wetland
455 soils controlled by organic matter mobility or Fe-oxyhydroxides reduction? *J. Colloid*
456 *Interface Sci.* 314(2), 490–501. <https://doi.org/10.1016/j.jcis.2007.04.062>

457 Hayakawa, C., Fujii, K., Funakawa, S., Kosaki, T., 2018. Effects of sorption on biodegradation
458 of low-molecular-weight organic acids in highly-weathered tropical soils. *Geoderma.* 324,
459 109–118. <https://doi.org/10.1016/j.geoderma.2018.03.014>.

460 Huang, Y., Zhao, L., Keller, A.A., 2017. Interactions, transformations, and bioavailability of
461 nano-copper exposed to root exudates. *Environ. Sci. Technol.* 51(17), 9774–9783.
462 <https://doi.org/10.1021/acs.est.7b02523>.

463 Huot, H., Simonnot, M.-O., Marion, P., Yvon, J., De Donato, P., Morel, J.-L., 2013.
464 Characteristics and potential pedogenetic processes of a Technosol developing on iron
465 industry deposits. *J. Soils Sediments.* 13(3), 555–568. [https://doi.org/10.1007/s11368-](https://doi.org/10.1007/s11368-012-0513-1)
466 [012-0513-1](https://doi.org/10.1007/s11368-012-0513-1).

467 Huot, H., Simonnot, M.-O., Watteau, F., Marion, P., Yvon, J., De Donato, P., et al., 2014. Early
468 transformation and transfer processes in a Technosol developing on iron industry deposits.
469 *Eur. J. Soil Sci.* 65(4), 470–484. <https://doi.org/10.1111/ejss.12106>.

470 Iwase, T., Varotsis, C., Shinzawa-Itoh, K., Yoshikawa, S., Kitagawa, T., 1999. Infrared
471 evidence for Cu B ligation of photodissociated CO of cytochrome c oxidase at ambient
472 temperatures and accompanied deprotonation of a carboxyl side chain of protein. *J. Am.*
473 *Chem. Soc.* 121(6), 1415–1416. <https://doi.org/10.1021/ja983242w>.

474 Jagadamma, S., Mayes, M.A., Phillips, J.R., 2012. Selective sorption of dissolved organic
475 carbon compounds by temperate soils. *PLoS One.* 7(11), e50434.
476 <https://doi.org/10.1371/journal.pone.0050434>.

477 Kanbar, H.J., Kaouk, M., 2019. Mineral and chemical changes of sediments after Cu sorption
478 and then desorption induced by synthetic root exudate. *Chemosphere.* 236, 124393.
479 <https://doi.org/10.1016/j.chemosphere.2019.124393>.

480 Kanbar, H.J., Srouji, E.E., Zeidan, Z., Chokr, S., Matar, Z., 2018. Leaching of metals in coastal
481 technosols triggered by saline solutions and labile organic matter removal. *Water, Air, Soil*
482 *Pollut.* 229(5), 157. <https://doi.org/10.1007/s11270-018-3808-z>.

483 Karageorgaki, C., Ernst, K.-H., 2014. A metal surface with chiral memory. *Chem. Commun.*
484 50(15), 1814–1816. <https://doi.org/10.1039/C3CC48797K>.

485 Lefevre, G.H., Hozalski, R.M., Novak, P.J., 2013. Root exudate enhanced contaminant

486 desorption: An abiotic contribution to the rhizosphere effect. *Environ. Sci. Technol.*
487 47(20), 11545–11553. <https://doi.org/10.1021/es402446v>.

488 Madejová, J., Gates, W.P., Petit, S., 2017. IR spectra of clay minerals. In: Gates, W.P.,
489 Klopogge, J.T., Madejová, J., Bergaya, F. (Eds.). *Developments in Clay Science*.
490 Eslevier, pp. 107–149. <https://doi.org/10.1016/B978-0-08-100355-8.00005-9>.

491 Markich, S.J., Brown, P.L., 1999. Thermochemical data for environmentally-relevant elements.
492 Australian Nuclear Science and Technology Organisation, Australian Nuclear Science and
493 Technology Organisation (ANSTO). E-report, Menai, Australia.

494 Matar, Z., Soares Pereira, C., Chebbo, G., Uher, E., Troupel, M., Boudahmane, L., et al., 2015.
495 Influence of effluent organic matter on copper speciation and bioavailability in rivers
496 under strong urban pressure. *Environ. Sci. Pollut. Res.* 22(24), 19461–19472.
497 <https://doi.org/10.1007/s11356-015-5110-6>.

498 Newcomb, C.J., Qafoku, N.P., Grate, J.W., Bailey, V.L., De Yoreo, J.J., 2017. Developing a
499 molecular picture of soil organic matter–mineral interactions by quantifying organo–
500 mineral binding. *Nat. Commun.* 8(1), 396. <https://doi.org/10.1038/s41467-017-00407-9>.

501 Oelkers, E.H., Golubev, S. V., Pokrovsky, O.S., Bénézech, P., 2011. Do organic ligands affect
502 calcite dissolution rates? *Geochim. Cosmochim. Acta.* 75(7), 1799–1813.
503 <https://doi.org/10.1016/j.gca.2011.01.002>.

504 Pan, B., Tao, S., Dawson, R.W., Xing, B.S., 2010. Formation of organo-mineral complexes as
505 affected by particle size, pH, and dry - wet cycles. *Soil Res.* 48(8), 713–719.
506 <https://doi.org/10.1071/SR10029>.

507 Pariyan, K., Hosseini, M.R., Ahmadi, A., Zahiri, A., 2019. Optimization and kinetics of oxalic
508 acid treatment of feldspar for removing the iron oxide impurities. *Sep. Sci. Technol.* 1–
509 12. <https://doi.org/10.1080/01496395.2019.1612913>.

510 Paz-Ferreiro, J., Lu, H., Fu, S., Méndez, A., Gascó, G., 2014. Use of phytoremediation and
511 biochar to remediate heavy metal polluted soils: A review. *Solid Earth.* 5(1), 65–75.
512 <https://doi.org/10.5194/se-5-65-2014>.

513 Perelomov, L. V., Pinskiy, D.L., Violante, A., 2011. Effect of organic acids on the adsorption
514 of copper, lead, and zinc by goethite. *Eurasian Soil Sci.* 44(1), 22–28.
515 <https://doi.org/10.1134/S1064229311010091>.

516 Song, Y., Ammami, M., Benamar, A., Mezazigh, S., Wang, H., 2016. Effect of EDTA, EDDS,
517 NTA and citric acid on electrokinetic remediation of As, Cd, Cr, Cu, Ni, Pb and Zn
518 contaminated dredged marine sediment. *Environ. Sci. Pollut. Res.* 23(11), 10577–10586.
519 <https://doi.org/10.1007/s11356-015-5966-5>.

520 Ström, L., Owen, A.G., Godbold, D.L., Jones, D.L., 2001. Organic acid behaviour in a
521 calcareous soil: Sorption reactions and biodegradation rates. *Soil Biol. Biochem.* 33(X),
522 2125–2133. [https://doi.org/10.1016/S0038-0717\(01\)00146-8](https://doi.org/10.1016/S0038-0717(01)00146-8).

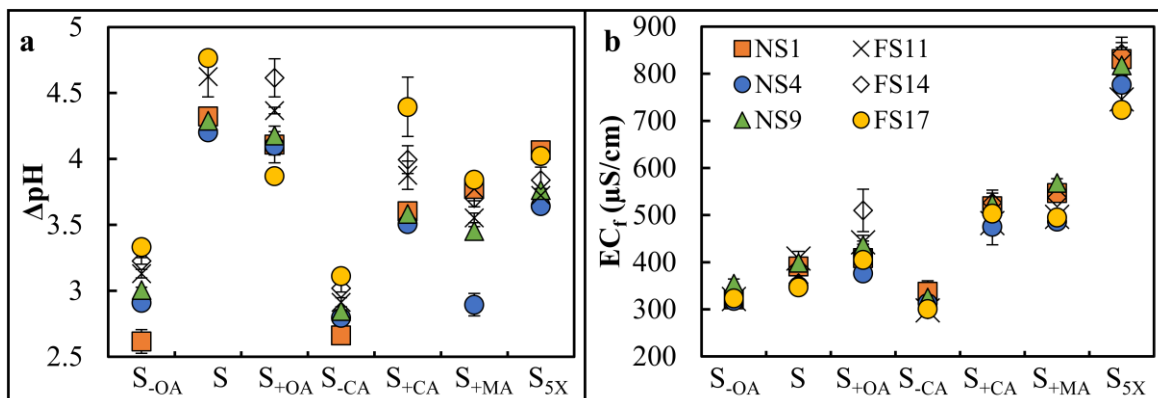
523 Van der Ent, A., Echevarria, G., Baker, A.J.M., Morel, J.L., (Editors), 2018. *Agromining:
524 Farming for Metals*. Springer Book. <https://doi.org/10.1007/978-3-319-61899-9>.

525 Violante, A., Caporale, A.G., 2015. Biogeochemical processes at soil-root interface. *J. Soil Sci.
526 Plant Nutr.* 15(2), 422–448. <https://doi.org/10.4067/s0718-95162015005000038>.

527

528

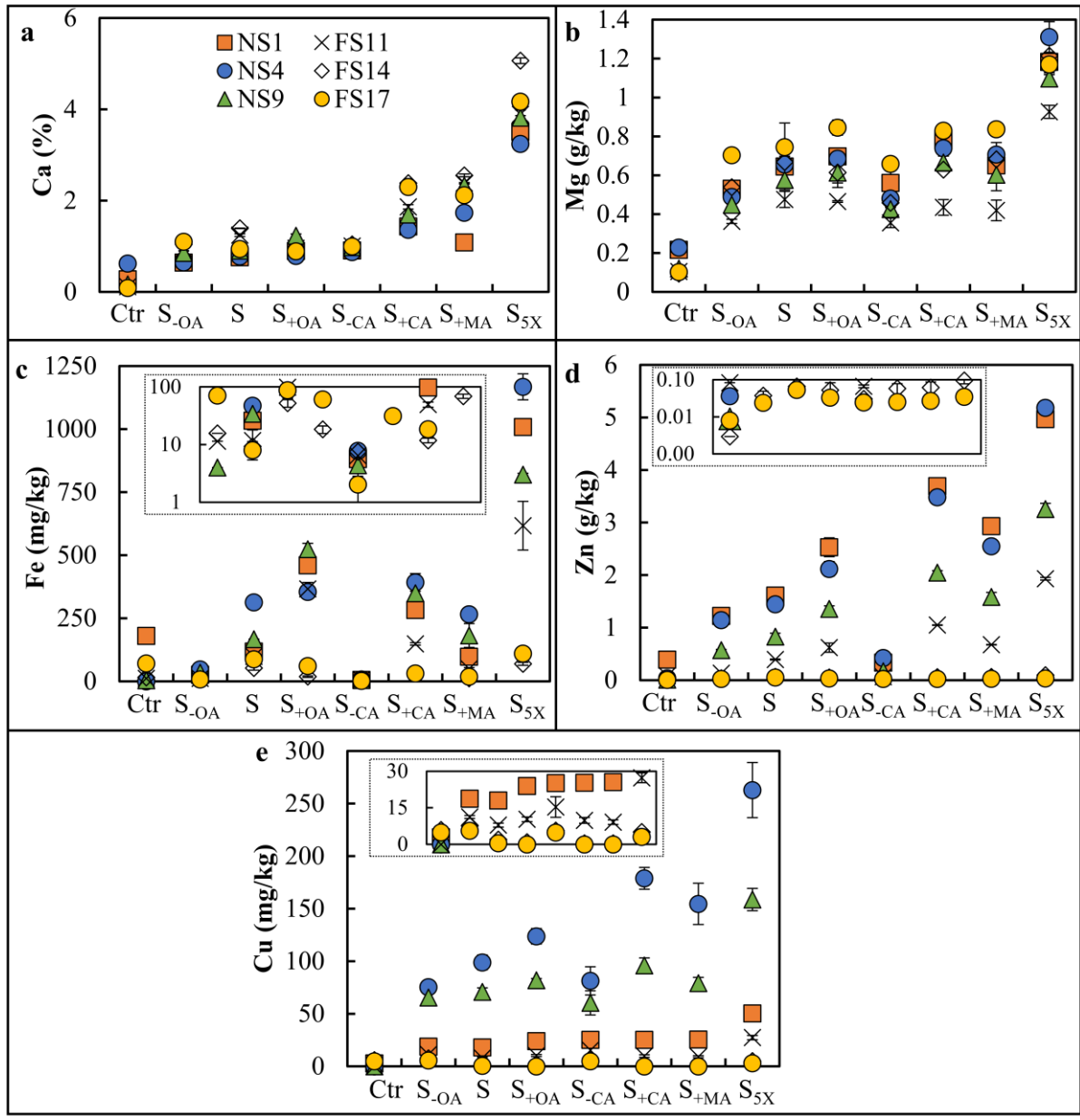
529 **List of figures**



530

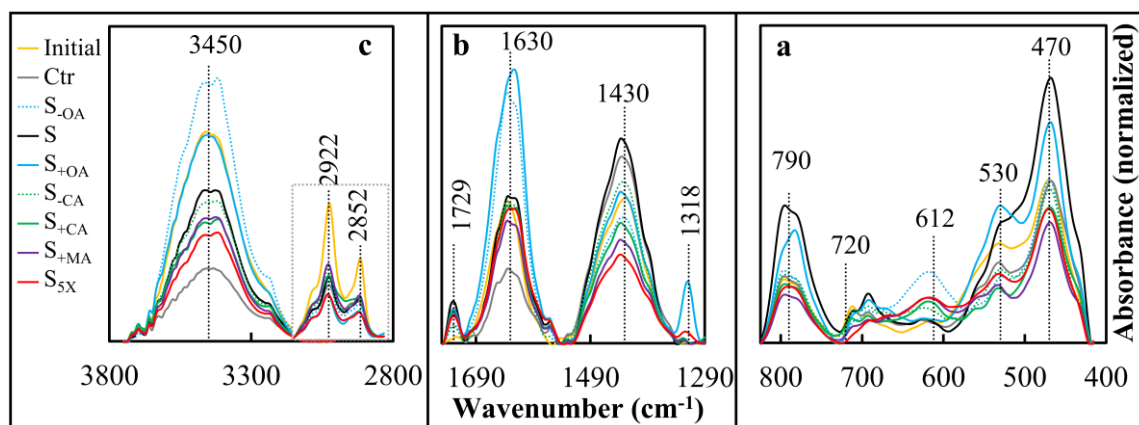
531

532 **Fig. 1** The variation of ΔpH (a) and EC_f (b) for the SRE solutions after mixing with the
 533 technosols. For a clearer representation of the graphs, the initial values are not included here;
 534 pH_i , pH_f , and EC_i are reported in **Table S2**.



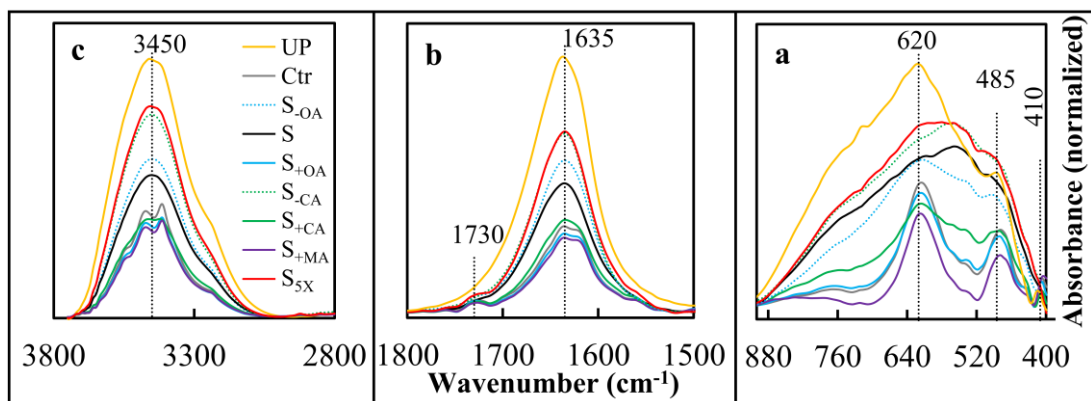
535
 536
 537
 538
 539

Fig. 2 The release of a) Ca (%), b) Mg (g/kg), c) Fe (mg/kg), d) Zn (g/kg), and e) Cu (mg/kg) from the technosols induced by SRE. The insets in c-e highlight the low metal release contents.

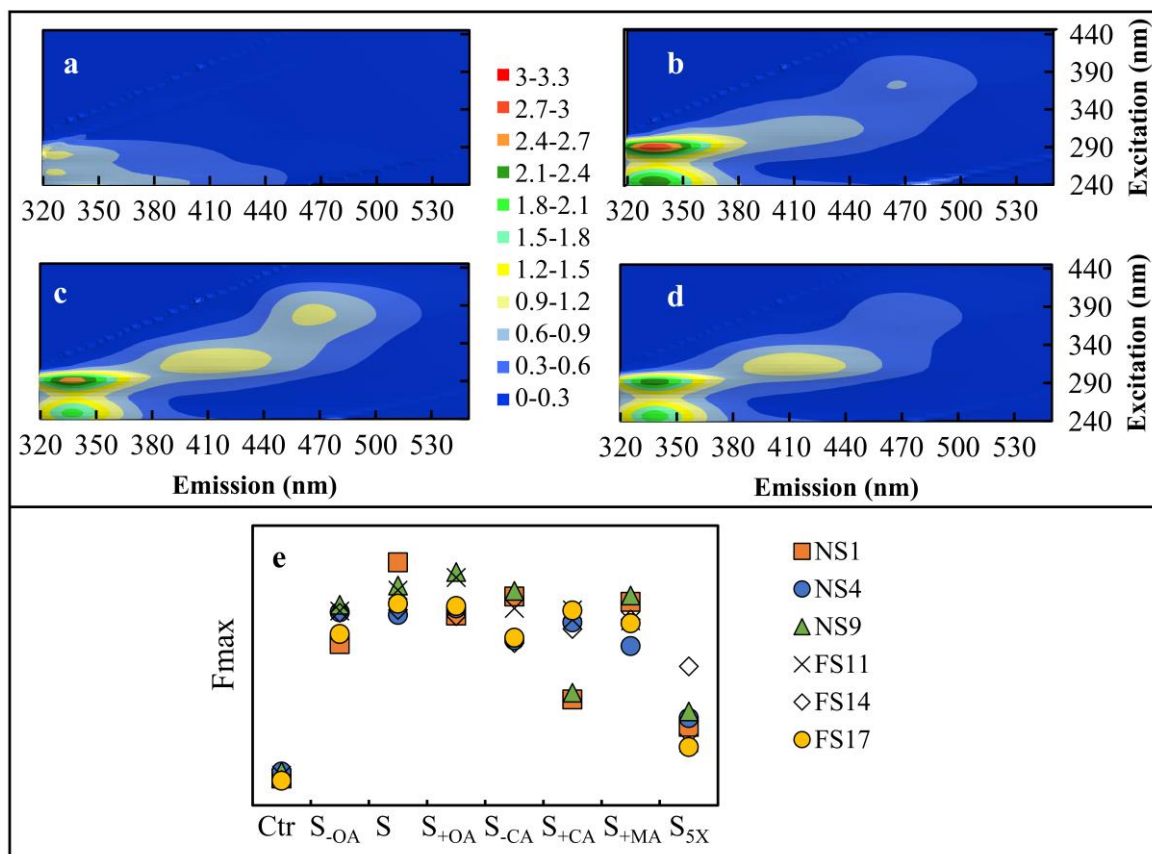


540
 541
 542
 543
 544
 545
 546

Fig. 3 FTIR spectra of the technosols after SRE treatments. The spectral regions are divided into 820-400 cm^{-1} (a), 1740-1290 cm^{-1} (b), and 3750-2800 cm^{-1} (c). The spectra in the 3000-2800 cm^{-1} region are enlarged for better visualization. For convenience, the spectra of only NS1 are included. Unless stated otherwise in the text, the other technosols showed similar changes.



547
 548 **Fig 4.** FTIR spectra of the liquid samples after the metal desorption experiment. The spectral
 549 regions are divided into 900-400 cm^{-1} (a), 1800-1500 cm^{-1} (b), and 3800-2800 cm^{-1} (c). For
 550 convenience, the spectra of only NS1 are included.
 551



552

553

554 **Fig 5.** Excitation-emission matrices (EEM) of the solutions after the metal sorption experiment

555 (a-d) and Fmax (e) for the second region (HA-like materials). The EEM of the control (a), S-0A

556 (b), S (c), and S+0A (d) treatments of NS1 are shown. The data for the other samples and

557 treatments are included in **Table S4**.

Appendix A. Supplementary data

Selective metal leaching from technosols based on synthetic root exudate composition

Hussein Jaafar Kanbar^{1,2,**}, Zeinab Matar^{1,3,4,**}, Ghina Safa^{1,3}, Veronique Kazpard^{1,3,4}

1. Research and Analysis Platform for Environmental Sciences (PRASE), Doctoral School of Sciences and Technology (EDST), the Lebanese University, P.O. 5, Rafic Hariri Campus, Hadat, Lebanon.
2. Department of Chemistry, Umeå University, SE-901 87, Umeå, Sweden.
3. Department of Earth and Life Sciences, Faculty of Sciences, the Lebanese University, Rafic Hariri Campus, Hadat, Lebanon.
4. Laboratory of Georesources, Geosciences and Environment (L2GE), Faculty of Sciences, the Lebanese University, Fanar, Lebanon.

Received 16 February 2020

Revised 13 April 2020

Accepted 24 April 2020

** These authors contributed equally to this work. Corresponding authors. E-mail: Hussein.kanbar@umu.se (H.J. Kanbar), z.matar@ul.edu.lb (Z. Matar).

 Hussein J. Kanbar <http://orcid.org/0000-0002-9505-9974>

Content

Table S1: The composition and concentrations of the synthetic root exudate components, and the structure and pKa values for the functional groups of the low molecular weight organic acids (LMWOAs).....	1
Table S2: The pH and EC (in $\mu\text{S}/\text{cm}$) values for the initial SRE solutions and the solutions after 24 hr mixing with technosols. The average values \pm standard deviations are included (n=3). For controls (Ctr, i.e., samples treated with ultrapure water), n=1	2
Table S3: Total metal content, oxalate extractable metal content, and percentage of oxalate extractable metals of the technosols (Kanbar et al., 2018).....	3
Table S4: Maximum fluorescence intensities (Fmax) for the SRE solutions after mixing with the technosols. Control indicates the technosols treated with ultrapure water.....	4
Fig. S1: Correlations between Mg and Ca release and electric conductivity “EC” (a) and the correlation between Zn, Cu, and Fe release (b-d)	5
Fig. S2: Ratios of metal release according to different treatments	6
S1: Quality assurance and quality control (QA/QC) procedures	7

Table S1: The composition and concentrations of the synthetic root exudate components, and the structure and pKa values for the functional groups of the low molecular weight organic acids (LMWOAs)

The concentrations included in the table are those in the SRE-technosol mixture. The concentrations that mark the variation between the different SRE solutions are highlighted in yellow.

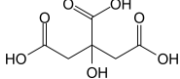
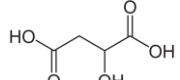
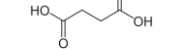
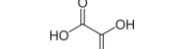
Component	Treatment							Structure	pKa (Kalka, 2019; Silva et al., 2009)	
	1	2	3	4	5	6	7		Group	Values
	S _{OA}	S	S _{+OA}	S _{-CA}	S _{+CA}	S _{+MA}	S _{5X}			
Concentrations (mmol/L) of the SRE components										
Sugar	Glucose.H ₂ O	0.5	0.5	0.5	0.5	0.5	0.5	2.5		
	D-Fructose	0.5	0.5	0.5	0.5	0.5	0.5	2.5		
	Sucrose	0.5	0.5	0.5	0.5	0.5	0.5	2.5		
Low molecular weight organic acids (LMWOAs)	Citric acid	0.25	0.25	0.25	0	1.25	0.25	1.25		Carboxyl pKa ₁ 3.1 pKa ₂ 4.8 pKa ₃ 6.4 Hydroxyl pKa 14.4
	Malic acid	0.25	0.25	0.25	0.25	0.25	1.25	1.25		Carboxyl pKa ₁ 3.4 pKa ₂ 5.2 Hydroxyl pKa 14.5
	Succinic acid	0.25	0.25	0.25	0.25	0.25	0.25	1.25		Carboxyl pKa ₁ 4.2 pKa ₂ 5.6
	Oxalic acid	0	0.25	1.25	0.25	0.25	0.25	1.25		Carboxyl pKa ₁ 1.3 pKa ₂ 4.3
	Sum of LMWOAs	0.75	1	2	0.75	2	2	5		
Amino acids	DL-Serine	0.125	0.125	0.125	0.125	0.125	0.125	0.625		
	L-Leucine	0.125	0.125	0.125	0.125	0.125	0.125	0.625		
	L-Proline	0.125	0.125	0.125	0.125	0.125	0.125	0.625		
Phenolic acid	Trans-Cinnamic acid	0.125	0.125	0.125	0.125	0.125	0.125	0.625		
	Vanillic acid	0.125	0.125	0.125	0.125	0.125	0.125	0.625		
	Trans-Ferulic acid	1.25	1.25	1.25	1.25	1.25	1.25	6.25		

Table S2: The pH and EC (in $\mu\text{S}/\text{cm}$) values for the initial SRE solutions and the solutions after 24 hr mixing with technosols. The average values \pm standard deviations are included (n=3). For controls (Ctr, i.e., samples treated with ultrapure water), n=1

Solution	Initial pH	pH of solutions after 24 hr						
		NS1	NS4	NS9	FS11	FS14	FS17	
Ctr	8.64	7.86	8.03	7.43	8.20	8.76	8.06	
Treatment	S _{OA}	6.07 \pm 0.09	6.36 \pm 0.03	6.46 \pm 0.02	6.58 \pm 0.03	6.68 \pm 0.02	6.78 \pm 0.02	
	S	7.45 \pm 0.03	7.33 \pm 0.05	7.42 \pm 0.03	7.76 \pm 0.16	7.89 \pm 0.01	7.90 \pm 0.01	
	S _{OA}	6.81 \pm 0.14	6.80 \pm 0.07	6.88 \pm 0.03	7.07 \pm 0.02	7.32 \pm 0.15	6.57 \pm 0.01	
	S _{CA}	6.27 \pm 0.05	6.41 \pm 0.02	6.46 \pm 0.01	6.52 \pm 0.03	6.63 \pm 0.03	6.72 \pm 0.00	
	S _{CA}	2.96	6.57 \pm 0.02	6.47 \pm 0.01	6.54 \pm 0.07	6.84 \pm 0.11	6.96 \pm 0.11	7.36 \pm 0.23
	S _{MA}	3.22	6.99 \pm 0.09	6.12 \pm 0.09	6.67 \pm 0.03	6.77 \pm 0.04	6.92 \pm 0.07	7.06 \pm 0.01
	S _{5X}	2.71	6.78 \pm 0.06	6.35 \pm 0.01	6.47 \pm 0.01	6.43 \pm 0.02	6.55 \pm 0.10	6.73 \pm 0.02

Solution	Initial EC ($\mu\text{S}/\text{cm}$)	EC ($\mu\text{S}/\text{cm}$) of solutions after 24 hr						
		NS1	NS4	NS1	FS11	NS1	FS17	
Ctr	80	102	131	109	72	71	76	
Treatment	S _{OA}	321 \pm 12	318 \pm 3	355 \pm 10	322 \pm 7	338 \pm 10	324 \pm 3	
	S	391 \pm 5	349 \pm 8	399 \pm 3	408 \pm 15	356 \pm 4	347 \pm 5	
	S _{OA}	409 \pm 29	376 \pm 6	436 \pm 9	442 \pm 15	510 \pm 45	405 \pm 8	
	S _{CA}	145	337 \pm 23	313 \pm 15	325 \pm 12	298 \pm 7	300 \pm 6	301 \pm 6
	S _{CA}	296	519 \pm 34	475 \pm 39	524 \pm 23	483 \pm 12	526 \pm 5	504 \pm 1
	S _{MA}	251	547 \pm 12	487 \pm 2	568 \pm 9	496 \pm 6	538 \pm 11	495 \pm 9
	S _{5X}	591	831 \pm 35	777 \pm 42	818 \pm 38	745 \pm 28	843 \pm 35	724 \pm 16

Table S3: Total metal content, oxalate extractable metal content, and percentage of oxalate extractable metals of the technosols (Kanbar et al., 2018)

Sample	Ca			Mg			Fe			Zn			Cu		
	Tot (%)	OxEx (%)	% Ox/Tot	Tot (%)	OxEx (%)	% Ox/Tot	Tot (%)	OxEx (%)	% Ox/Tot	Tot (mg/kg)	OxEx (mg/kg)	% Ox/Tot	Tot (mg/kg)	OxEx (mg/kg)	% Ox/Tot
NS1	11.6	-	-	2.9	0.3	9.1	12.3	5.7	45.9	22143	12463	56	434	263	61
NS4	9.6	-	-	2.7	0.2	7.7	20.0	16.0	79.8	12562	7897	63	2745	1023	37
NS9	8.5	-	-	0.4	0.2	41.0	23.7	16.9	71.0	15391	8701	57	3060	848	28
FS11	10.9	-	-	0.9	0.6	63.6	3.6	2.9	80.8	6018	5329	89	159	87	54
FS14	9.7	-	-	0.9	0.5	49.6	3.4	0.5	15.6	459	267	58	28	16	57
FS17	3.1	-	-	0.7	0.1	20.6	5.4	0.3	5.7	87	67	78	28	8	27

Tot: total metal content
OxEx: oxalate extractable metal content
% Ox/Tot: the percentage of oxalate extractable metal divided by the total metal multiplied by 100.

The bold characters highlight % Ox/Tot of samples with the highest metal release (more information is found in the main text). Ferriallophanes are identified by high oxalate extractable Fe out of total Fe contents (i.e., high % Ox/Tot).

Table S4: Maximum fluorescence intensities (Fmax) for the SRE solutions after mixing with the technosols. Control indicates the technosols treated with ultrapure water

Sample	Treatment	1 st region		2 nd region
		Peak1	Peak2	Peak3
		$\lambda_{ex}/\lambda_{em} = 245-$ 250/338 nm	$\lambda_{ex}/\lambda_{em} = 290-$ 295/338 nm	$\lambda_{ex}/\lambda_{em} = 260-$ 420/380-500 nm
NS1	Control	800	936	241
	S-OA	2352	3006	1016
	S	1892	2596	1797
	S+OA	1969	2299	1376
	S-CA	1334	1238	1596
	S+CA	2228	2706	634
	S+MA	1733	2072	1487
	S _{5X}	77	60	489
NS4	Control	1391	1510	303
	S-OA	2661	3223	1301
	S	1408	2074	1328
	S+OA	2766	3807	1441
	S-CA	1767	1567	1204
	S+CA	1332	1987	1322
	S+MA	1606	3304	1092
	S _{5X}	31	22	568
NS9	Control	1949	2047	301
	S-OA	2118	2169	1366
	S	1976	2221	1589
	S+OA	2380	2843	1763
	S-CA	1393	1530	1644
	S+CA	1711	2490	693
	S+MA	1157	1308	1543
	S _{5X}	106	91	625
FS11	Control	1841	1942	268
	S-OA	1691	1589	1309
	S	1853	1813	1546
	S+OA	1875	1920	1715
	S-CA	1834	1706	1488
	S+CA	1515	1783	1432
	S+MA	1469	1629	1316
	S _{5X}	54	44	344
FS14	Control	2376	2382	227
	S-OA	2865	2235	1295
	S	2130	2102	1369
	S+OA	1699	1566	1369
	S-CA	1136	1025	1179
	S+CA	1227	1233	1262
	S+MA	1438	1372	1327
	S _{5X}	80	59	1027
FS17	Control	464	721	222
	S-OA	1787	1893	1106
	S	1784	1941	1427
	S+OA	1818	1649	1462
	S-CA	1370	1260	1227
	S+CA	2054	2173	1430
	S+MA	1414	1466	1295
	S _{5X}	127	92	309

Fig. S1: Correlations between Mg and Ca release and electric conductivity “EC” (a) and the correlation between Zn, Cu, and Fe release (b-d)

The change in EC was mainly dependent on the release of the major cations (Ca and Mg), as seen by strong correlations between each metal and EC (R^2 values in part “a” of the figure). Furthermore, the release of Mg and Ca is strongly correlated to the concentrations of the low molecular weight organic acids (LMWOAs) in the synthetic root exudate (SRE) solutions. On the other hand, the release of Fe, Zn, and Cu largely depended on the technosols (and less on the SRE solution). For example, Cu-Fe and Cu-Zn were correlated between two groups of technosols, which are NS4-NS9 and the other samples (NS1 and FS technosols). As for Zn-Fe, they were correlated between two other groups, which are all the NS samples and FS11 (group 1) and FS14 and FS17 (group 2). This highlights that in addition to the role of LMWOAs, metal behavior is largely dependent on the characteristics of technosols.

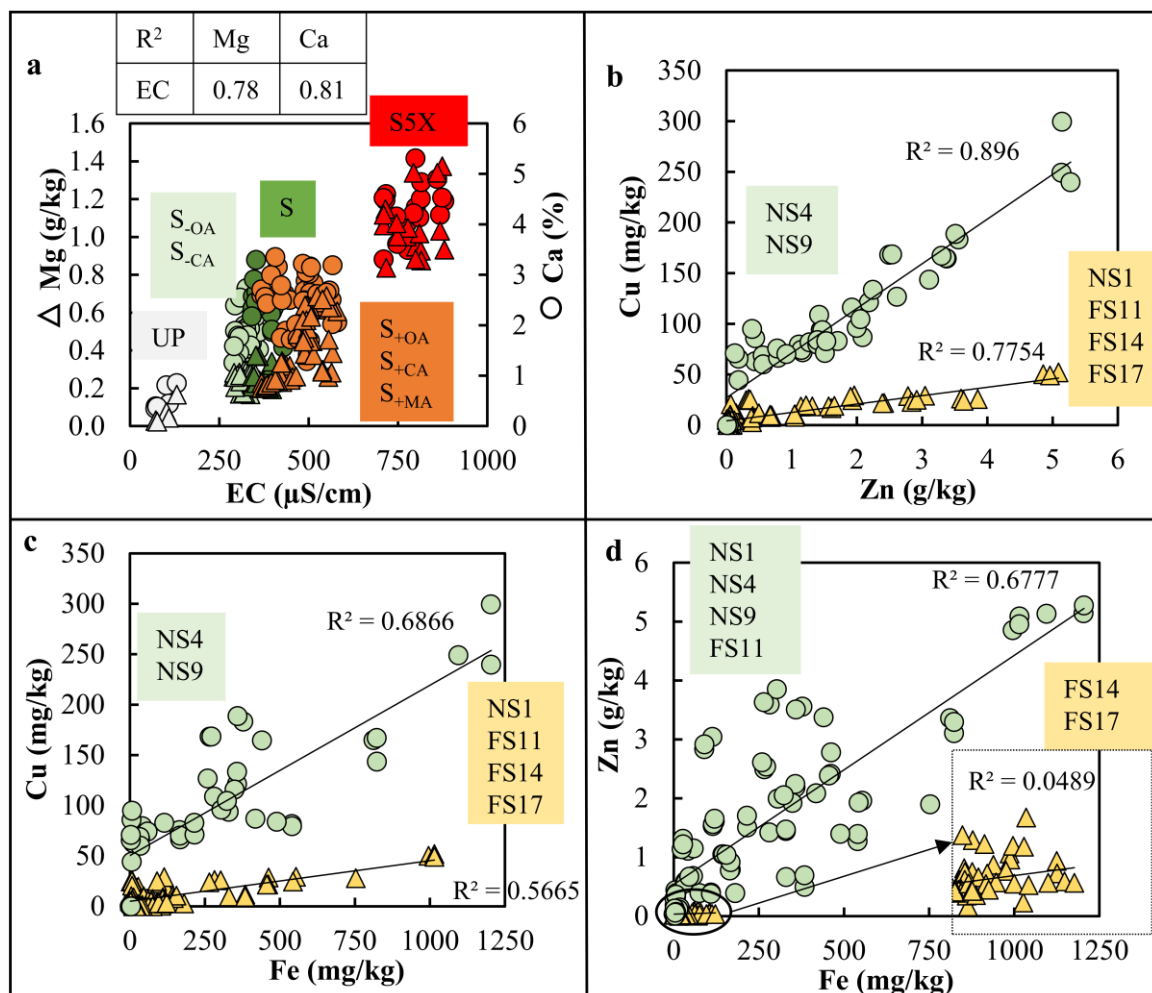
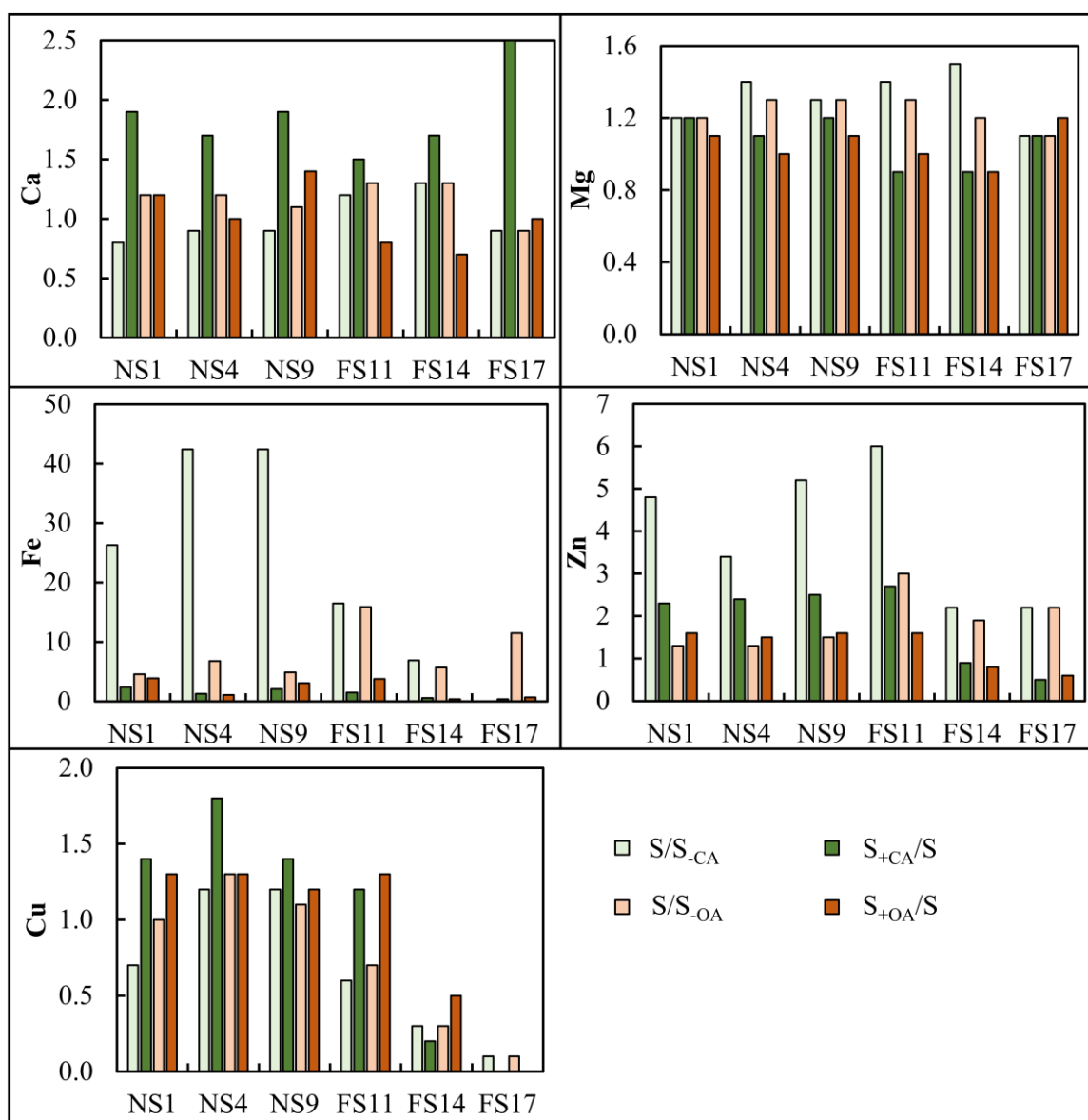


Fig. S2: Ratios of metal release according to different treatments

Ratios of metal release were used for a clearer visualization of the link between the influence of low and high concentrations of LMWOAs. For example, S/S_{-CA} highlighted the role of relatively low concentrations of CA (0-0.25 mmol/L) and S_{+CA}/S highlighted the role of relatively high concentrations of CA (0.25-1.25 mmol/L). In the case of Zn, $Zn\ S/S_{-CA} > S_{+CA}/S$. So, Zn release by SRE was more prominent when CA concentrations were relatively low; under higher concentrations of CA (0.25-1.25 mmol/L), Zn release was less prominent.



S1: Quality assurance and quality control (QA/QC) procedures

QA/QC procedures were implemented based on external standards. Those standards were also used for calibration. Accuracy and reproducibility of the measurements were validated by running the external standards between every ~10 samples. The values were taken unless the error exceeded 5-10%. The quantification and detection limits (LOQ and LOD, respectively) were calculated according to the ICH Harmonized Tripartite Guideline (ICH Harmonized Tripartite Guideline, 2005).

References

- ICH Harmonized Tripartite Guideline, 2005. Validation of analytical procedures: text and methodology Q2 (R1), in: International Conference on Harmonization of Technical Requirements for Registration of Pharmaceuticals for Human Use. Geneva, Switzerland, p. 13.
- Kalka, H., 2019. Organic Acids and Salts [WWW Document]. Aqion. URL <https://www.aqion.de/site/189#pK> (accessed 12.14.19).
- Kanbar, H.J., Srouji, E.E., Zeidan, Z., Chokr, S., Matar, Z., 2018. Leaching of metals in coastal technosols triggered by saline solutions and labile organic matter removal. *Water, Air, Soil Pollut.* 229, 157. <https://doi.org/10.1007/s11270-018-3808-z>
- Silva, A.M.N., Kong, X., Hider, R.C., 2009. Determination of the pKa value of the hydroxyl group in the α -hydroxycarboxylates citrate, malate and lactate by ^{13}C NMR: implications for metal coordination in biological systems. *BioMetals* 22, 771–778. <https://doi.org/10.1007/s10534-009-9224-5>